Acoustic Emission and Low Temperature Calorimetry Study of Freeze and Thaw Behavior in Cementitious Materials Exposed to NaCl Salt

Yaghoob Farnam
Graduate Research Assistant, Ph.D. Student,
School of Civil Engineering, Purdue University,
550 Stadium Mall Drive,
West Lafayette, IN 47907, USA,
Email: yfarnam@purdue.edu
Phone: +1-765-543-0269

Dale Bentz
Chemical Engineer,
Materials and Structural Systems Division,
National Institute of Standards and Technology,
100 Bureau Drive, Stop 8615,
Gaithersburg, MD 20899, USA,
Email: dale.bentz@nist.gov
Phone: +1-301-975-5865

Allison Hampton
Undergraduate Research Assistant,
School of Civil Engineering, Purdue University,
550 Stadium Mall Drive,
West Lafayette, IN 47907, USA,
Email: ahampto@purdue.edu
Phone: +1-765-337-5056

and

Jason Weiss
(Corresponding Author)
Professor, Director of Pankow Materials Laboratory,
School of Civil Engineering, Purdue University,
550 Stadium Mall Drive,
West Lafayette, IN 47907,
Email: wjweiss@purdue.edu
Phone: +1-765-494-2215

ABSTRACT

This paper describes a series of experiments that were performed to assess the freeze-thaw behavior of mortar specimens exposed to NaCl solutions. A low-temperature longitudinal guarded comparative calorimeter was used to perform cyclic freeze-thaw testing on mortar specimens saturated with NaCl solutions. Heat flow and acoustic emission activity were monitored during the freeze-thaw experiment to detect ice formation and cracking. Although the conventional water-NaCl phase diagram would suggest that no freezing or damage would occur in specimens saturated with 15 % and 23.3 % NaCl solution by mass within the applied freeze-thaw temperature range, damage was observed. For these specimens, an additional heat flow peak attributed to an unexpected phase change, accompanied by acoustic activity, was detected at a temperature higher than the expected freezing point. To better understand the source of this damage, a low temperature differential scanning calorimeter was used to investigate the influence of NaCl on freeze-thaw behavior of water, two pore solutions, hydrated cement powder, and calcium hydroxide powder. The results showed that the pore solution alters the freeze-thaw behavior slightly; however, it does not exhibit the unexpected phase change at higher concentrations. The specimens made with hydrated cement powder showed the unexpected phase change in high concentrations of NaCl solution in a temperature range between 0 °C and 8 °C. While the exact nature of this phase change is not definitively known, it appears that it results in premature damage during freeze-thaw when high concentration salt solutions are used, even if freezing of the solution is not occurring.

INTRODUCTION

Deicing salts are widely used on concrete pavements and bridge decks to depress the freezing temperature of water and improve safety for the travelling public. Although the addition of deicing salts on the surface of concrete can melt the ice and increase the safety of the infrastructure, it can also cause premature deterioration of concrete, scaling, damage in pavement joints, and corrosion of reinforcing steel, as many deicing salts contain chlorides *(1–4)*. A variety of complex damage mechanisms can occur for concretes exposed to freeze-thaw and deicing salts. Formation of ice inside the concrete pore structure can cause hydraulic pressure *(5)* or osmotic pressure resulting from the partial freezing of solutions in capillaries *(6)*. In addition, the crystallization of salt *(7, 8)*, formation of Friedel's/Oxychloride/Kuzel's salt *(9–12)*, or changing the microstructure of hydration products *(11, 13, 14)* can be different sources of deterioration in concrete under freeze-thaw exposure. Deicing salts can also change the pore solution properties and cement hydration products, thereby inducing the formation of different phases. While a conventional interpretation of the aqueous NaCl phase diagram dictates that using a higher concentration of salts can prevent freezing (thereby resulting in almost no damage), these complex damage mechanisms can cause severe deterioration even as the concrete temperature varies above the liquidus line (Figure 1).

The main objective of this study is to determine the freeze-thaw behavior of cementitious materials when they are exposed to NaCl deicing salt. To understand the complex damage mechanisms and to evaluate possible chemical/physical sources, acoustic emission (AE) and calorimetry techniques were used in this study. AE techniques have been proven capable of quantifying the damage caused by freeze-thaw cycles in concrete *(15–21)*. Calorimetry studies have also been used to investigate phase transformations of water and NaCl solution in hardened cement paste *(22–24)*. When one phase transforms into another phase, latent heat must either be released or absorbed *(22, 25)*; the amount of latent heat and related temperatures are specific material properties that can be used to distinguish different materials or phases in a composite system. Thereby, the possible freeze-thaw damage sources due to any phase change can be defined. In the present study, in addition to AE measurement, a low temperature longitudinal guarded comparative calorimeter (LGCC) *(21)* was used to quantify the heat flow and thermal properties of mortar specimens. A low temperature differential scanning calorimeter (LT-DSC) was also used to investigate phase transformations and to detect the possible freeze-thaw damage source.

EXPERIMENTAL PROGRAM

Materials, Mixture Proportioning, and Specimen Preparation

Ordinary Type I portland cement (OPC) with a Blaine fineness of 375 m^2/kg was used in this study. The chemical composition of this cement reported by production manufacture is indicated in Table 1. Aggregates used to prepare mortar specimens consisted of natural sand with a maximum size of 4.75 mm, specific gravity of 2.61, fineness modulus of 2.89, and an absorption value of 2.2 % by mass. A single mortar mixture was used with a sand volume fraction of 55 % and a water-to-cement ratio (*w/c*) of 0.42 by mass. No chemical admixtures or supplementary cementitious materials were used. For cement paste specimens, the *w/c* was 0.42.

123 **TABLE 1 Properties of Ordinary Type I Portland Cements (OPC)**

Item	Percent by mass (%)
Silicon Dioxide (SiO_2)	19.43
Aluminum Oxide (Al_2O_3)	5.39
Ferric Oxide (Fe_2O_3)	3.18
Calcium Oxide (CaO)	63.45
Magnesium Oxide (MgO)	2.97
Sulfur Trioxide (SO_3)	3.38
Loss on Ignition	0.88
Sodium Oxide	0.35
Potassium Oxide	0.77
Insoluble Residue	0.25
Total Equivalent Alkali as Na_2O	0.86
Tricalcium Silicate (C_3S)	60
Dicalcium Silicate (C_2S)	10
Tricalcium Aluminate (C_3A)	9
Tetracalcium Aluminoferrite (C_4AF)	10

125

126   For the LGCC and AE experiment, specimens were prepared in a standard mortar mixer
127 in accordance with ASTM C305-12 *(26)*. The mortar was cast in 25.4 mm × 25.4 mm × 300 mm
128 (1 in × 1 in × 11.81 in) molds that were demolded after 24 h. All mortar bars were then sealed in
129 double plastic bags and cured for 28 d in these sealed conditions at 23 °C ± 0.5 °C. After 28 d of
130 curing, the mortar bars were cut using a wet saw to 25.4 mm × 25.4 mm × 50.8 mm (1 in × 1 in ×
131 2 in) specimens. These specimens were then placed in a vacuum oven at 65 °C ± 1 °C and a
132 pressure of 20 mm Hg ± 5 mm Hg for 7 d. While ASTM C1645-11 *(27)* suggests using a 3 %
133 NaCl solution, higher range of NaCl concentration was used in this study. Solutions with an
134 initial concentration of 0 %, 5 %, 15 %, and 23.3 % by mass NaCl were used to vacuum saturate
135 the mortar specimens. After vacuum saturation, the specimens were transferred to a 23 °C ± 0.5
136 °C chamber before testing, where they were kept in a container submerged in solution for 3 d.
137 This condition was considered as fully saturated (i.e., assuming 100 % degree of saturation).
138 After conditioning, specimens were wrapped with a very thin plastic sheet to protect them from
139 subsequent moisture exchange with their surrounding environment (minimizing their absorption
140 or release of water) during the freeze-thaw process. The top and bottom cross section plastic
141 covers were removed to ensure a better connection with thermal pads during the freeze-thaw
142 tests. In addition, a small circular hole was made in the side plastic of each specimen to attach
143 the AE sensor.
144   For the LT-DSC study, five series of tests were performed: 1) water-NaCl, 2) low alkali
145 pore solution-NaCl, 3) high alkali pore solution-NaCl , 4) water-NaCl-Ca(OH)$_2$, and 5) water-
146 NaCl-Cement powder. NaCl with a purity of 99.9 % and de-ionized water were used to prepare
147 solutions. Series 2 and 3 were prepared with simulated pore solution instead of water. For the
148 first pore solution (i.e., low alkali), KOH and NaOH were used to make a solution with [K^+],
149 [Na^+], and [OH^-] of 0.65, 0.45, and 1.10 mol/liter, respectively. This was calculated using
150 software for estimation of pore solution properties developed previously
151 (http://concrete.nist.gov/poresolncalc.html) *(28)* corresponding to the cement used in this study,
152 considering 100 % degree of hydration in a sealed condition. For the second pore solution (i.e.,
153 high alkali), [K^+], [Na^+], and [OH^-] of 0.91, 0.62, and 1.53 mol/liter, respectively, were prepared
154 to have an equivalent alkali (as Na_2O) of 1.2 % by mass. Different percentages of NaCl salt were
155 added to the pore solution with respect to the corresponding mass of de-ionized water. Series 4
156 was like Series 1, however calcium hydroxide (Ca(OH)$_2$) powder was also used. For powder

specimens, the NaCl solutions were prepared and mixed with the powder just before LT-DSC testing.

For series 5, cement paste specimens were cast in a plastic container and cured for one year in a sealed condition. After, the specimen was ground using a grinder. The hydrated cement powder was stored in a vacuum oven at 65 °C ± 1 °C and a pressure of 20 mm Hg ± 5 mm Hg for 3 d to remove moisture.

Testing Design and Procedure

Acoustic Emission Low Temperature Longitudinal Guarded Comparative Calorimeter (AE-LGCC)

Mortar specimens saturated with de-ionized water and salt solutions (0 %, 5 %, 15 %, and 23.3 % NaCl by mass) were prepared for freeze-thaw testing. For each concentration, one specimen was used to perform the freeze-thaw test. A low temperature AE-LGCC was used to perform the freeze-thaw experiments. A temperature gradient was established in the test specimen by a two-stage cold plate. To produce a one-dimensional heat flow, heat losses in lateral directions were minimized by using a longitudinal guard and thermal insulation. Temperatures at different locations of the specimen and meter bars were recorded during freeze-thaw testing. A test specimen was inserted between two 25.4 mm × 25.4 mm × 25.4 mm (1 in × 1 in × 1 in) Pyroceram Code 9606[1] meter bars with known thermal properties. The experimental setup is illustrated in Figure 1b. Knowing the thermal properties of the meter bar, heat flow in the top and the bottom Pyroceram can be calculated using Equations 1, 2, and 3. The heat flow consumed or released by the mortar specimen (i.e., heat flow inward or outward specimen) can also be estimated by Equation 4:

$$\lambda_{PC} = -0.0061(T) + 4.2013 \qquad\qquad -50\,°C < T < 30\,°C \qquad (1)$$

$$q_T = \lambda_{PC}.\frac{T_6 - T_7}{d_{PC}} \qquad (2)$$

$$q_B = \lambda_{PC}.\frac{T_2 - T_3}{d_{PC}} \qquad (3)$$

$$\Delta Q_{Sample} = (q_B - q_T).A \qquad (4)$$

where λ_{PC} is thermal conductivity (W/(m•K)) of Pyroceram at its average temperature, q_T and q_B are respectively heat flow per unit area (W/m^2) through the top and bottom Pyroceram meter bars, d_{PC} and A are respectively the thickness of the Pyroceram meter bar (m) and cross-sectional area of the specimen (m^2), and T_i is the temperature (°C) measured by thermocouple at location i (shown in Figure 1b).

To quantify the damage caused by freeze and thaw cycles in the specimens, acoustic emission (AE) techniques were used. These techniques can typically be classified as either active acoustic emission (measuring wave speed using a pulsed wave) or passive acoustic emission (listening for waves generated due to cracking during freezing or thawing). In this study, passive and active acoustic emission techniques were used to measure the freeze-thaw activity/damage

---

[1] Certain commercial products are identified in this paper to specify the materials used and procedures employed. In no case does such identification imply endorsement or recommendation by the National Institute of Standards and Technology, or Purdue University, nor does it indicate that the products are necessarily the best available for the purpose.

along with the LGCC. One broadband sensor was attached to the specimen to record acoustic activity during the freeze-thaw test, while two coupled AE sensors were used to perform pulse velocity measurement through the length of the specimen before and after the freeze-thaw test. These AE-LGCC protocols have been well described in previous work *(21)*.

Figure 1a is a phase diagram of aqueous NaCl. The phase diagram is often used to describe the effectiveness of deicing salt (by % mass) on depressing the solution freezing temperature (i.e., liquidus line). The phase diagram can be described by three paths (shown in Figure 1a) to show the different freeze-thaw responses that would be expected. Path 1 describes a temperature change from +15 °C to -27 °C; decreasing the temperature from + 15 °C causes no change in solution until the temperature goes below the liquidus line. At this point, pure ice begins to form in the solution and the concentration of unfrozen solution increases. Decreasing the temperature further causes the ice mass fraction to increase which is accompanied by increasing the concentration of the unfrozen solution. This action continues as the temperature decreases until it reaches the eutectic temperature (-21.1 °C). Below this temperature, just two phases are present including ice and the eutectic phase containing ice and $NaCl \cdot 2H_2O$ crystals (hydrohalite). The opposite action occurs when heating is applied to the system. When the temperature rises to -21.1 °C, the eutectic phase melts and as the temperature rises further, ice gradually melts into solution, thereby decreasing the solution concentration. When the temperature reaches the liquidus point, all of the ice converts to liquid. It should be mentioned that in the cooling process, undercooling is often seen and the phase transition occurs at a lower temperature than that expected from the equilibrium NaCl phase diagram.

Path 2 and path 3 show a smaller range of temperature variation from +10 °C to -12 °C as is applied to the specimen for the freeze-thaw test in this study. For the lower concentration of NaCl, path 2 passes the liquidus line inducing the formation of ice; however, the temperature does not reach as low as the eutectic temperature. Therefore, ice is formed and can cause expansion and damage to mortar specimens. However, if the higher concentration of NaCl solution is used, no phase change is expected to occur in the range of applied temperature i.e., it is above the liquidus line (path 3).

In this study, three cycles of freeze-thaw were applied to the specimen. Temperature was controlled by the two-stage cold plate to vary from +10 °C to -14 °C. Figure 2c shows the temperature profile of the cold plate for this test. The temperature on the bottom surface of the mortar specimen (coldest part) was found to be between +10 °C and -12.5 °C. It has also been shown that the solution in a cementitious porous material freezes and ice propagates at 4 °C to 7 °C below its freezing point, due to undercooling, capillary pressure, and the pore size distribution *(21, 29)*. Therefore, it is expected to have almost no freezing for specimens saturated with 15 % and 23.3 % NaCl solution in the temperature range applied herein for freeze-thaw testing.

Low Temperature Differential Scanning Calorimetry (LT-DSC)

LT-DSC measures the temperatures and heat flows associated with phase transitions (and reactions) in materials as a function of temperature or time in a controlled low temperature atmosphere. This technique provides quantitative and qualitative information about physical and chemical changes that involve endothermic or exothermic processes. In the present research, a LT-DSC instrument (TA Q2000[1]) with an operating range of -90 °C to 550 °C was used to study low temperature phase transitions. Five different systems were studied. In the first series, NaCl solutions with different mass fractions of NaCl salt and deionized water were tested. In the

second and third series of study, the deionized water from series one was replaced with low
alkali and high alkali pore solutions. In the fourth and fifth series, calcium hydroxide and powder
of hydrated cement were used with the addition of different NaCl solutions. For series 1 to 3, a
total solution mass of 3 mg to 5 mg was used in LT-DSC, while for series 4 and 5, 9 mg to 11
mg of powder was mixed with 9 mg to 11 mg of solution and was tested at three ages after
mixing with NaCl solution: immediately after mixing (0 d), 1 d after mixing, and 7 d after
mixing. For LT-DSC experiments, one specimen was tested for each solution concentration.

For series 1, aluminum hermetic pans were used while for the rest of the experiments,
high volume stainless steel hermetic pans were used. Aluminum hermetic pans and high-volume
specimen pans are designed to accommodate 40 µL and 100 µL specimen sizes, an internal
pressure capability of 300 kPa and 3.7 MPa, and to withstand the temperature limits of -180 °C
to 600 °C and -100 °C to 250 °C, respectively. In this study, a cooling/heating temperature range
of 25 °C to -80 °C was performed on all specimens with a cooling and heating rate of 5 °C/min.
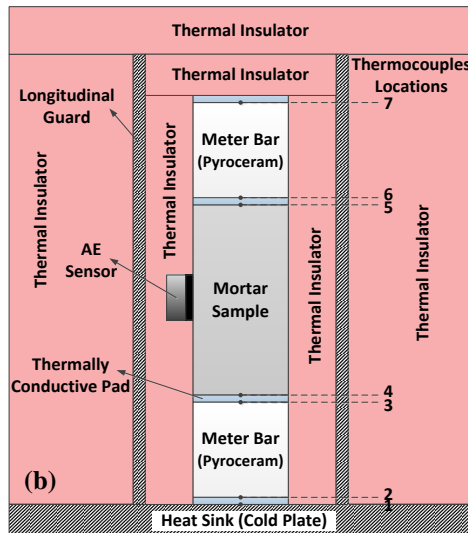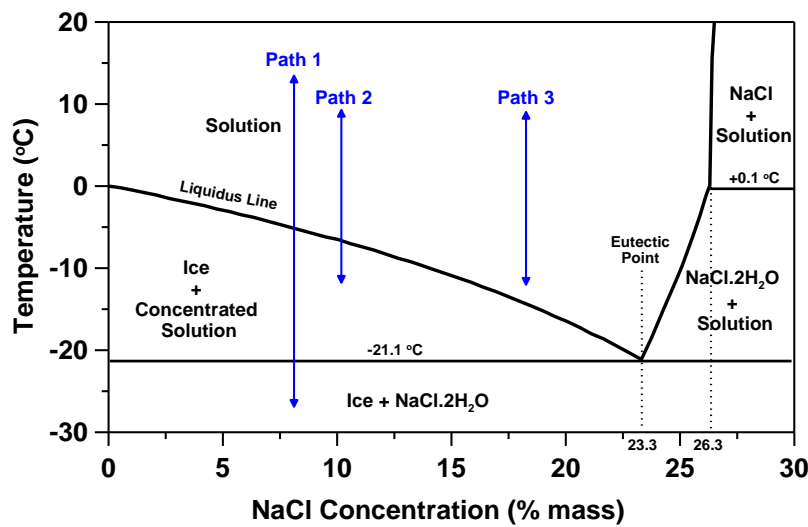

(a)

(b)

(c)
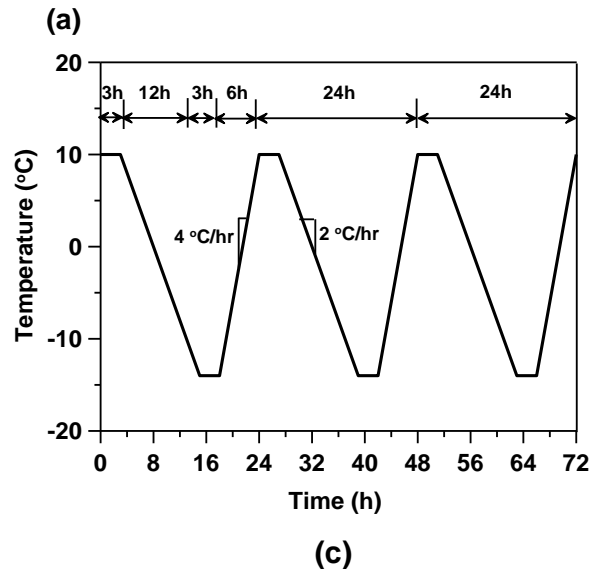
FIGURE 1 a) Phase diagram of aqueous NaCl, b) schematic of mortar specimen inserted between Pyroceram
meter bars inside LGCC with AE sensor *(21)*, and c) temperature profile of cold plate used for freeze-thaw
testing.

RESULTS AND DISCUSSION

Acoustic Emission Low Temperature Longitudinal Guarded Comparative Calorimeter (AE-LGCC)

Temperature and AE activity are plotted as a function of time for specimens saturated with de-ionized water, 5 %, 15 %, and 23.3 % NaCl in Figure 2. For specimens saturated with de-ionized water, 15 %, or 23.3 % NaCl solution, a lower number of AE events are recorded in comparison to the specimen containing 5 % NaCl solution. The acoustic events begin to occur as the temperature of the specimen decreases. A cluster of acoustic events is shown in Figure 2b and 2d as highlighted by the ellipsoid in the first freeze-thaw cycle. This cluster of data is not seen in the second and third cycle. These events can be attributed to microcracking of the specimen because of the thermal expansion coefficient mismatch between the paste and aggregate. Because the thermal loading is repeated during the second and third cycle, the damage attributed to thermal expansion coefficient mismatch does not appear in the subsequent cycles *(15)*.

As indicated in Figure 2b and 2d, a greater number of AE events were observed for specimens saturated by de-ionized water and 5 % of NaCl solution during freezing (i.e., ice formation) in comparison to other specimens. In addition to AE activity during freezing, another cluster of AE activity was seen during thawing. For specimens saturated by 15 % and 23.3 % NaCl solution, a less substantial amount of acoustic activity was observed in the specimen (Figure 2f and 2h), as the freezing points for 15 % and 23.3 % NaCl solution (with undercooling effects) are lower than the applied minimum temperature at the bottom surface of the mortar specimen (i.e., -12.5 °C). However, a cluster of AE activity was still seen (Figure 2f and 2h), while it was expected to have almost no AE activity for these specimens. In addition, as shown in Figure 2e, 2f, 2g, and 2h, an unexpected temperature jump (or phase change) was seen at a temperature greater than the expected freezing point (liquidus point) in the aqueous NaCl phase diagram. It was observed that AE events also accompanied this phase change and ended when the heating process was applied. This activity would not correspond to ice formation. For specimen saturated by 23.3 % NaCl solution, very little AE activity was observed during the first cycle while AE events were seen for subsequent cycles.
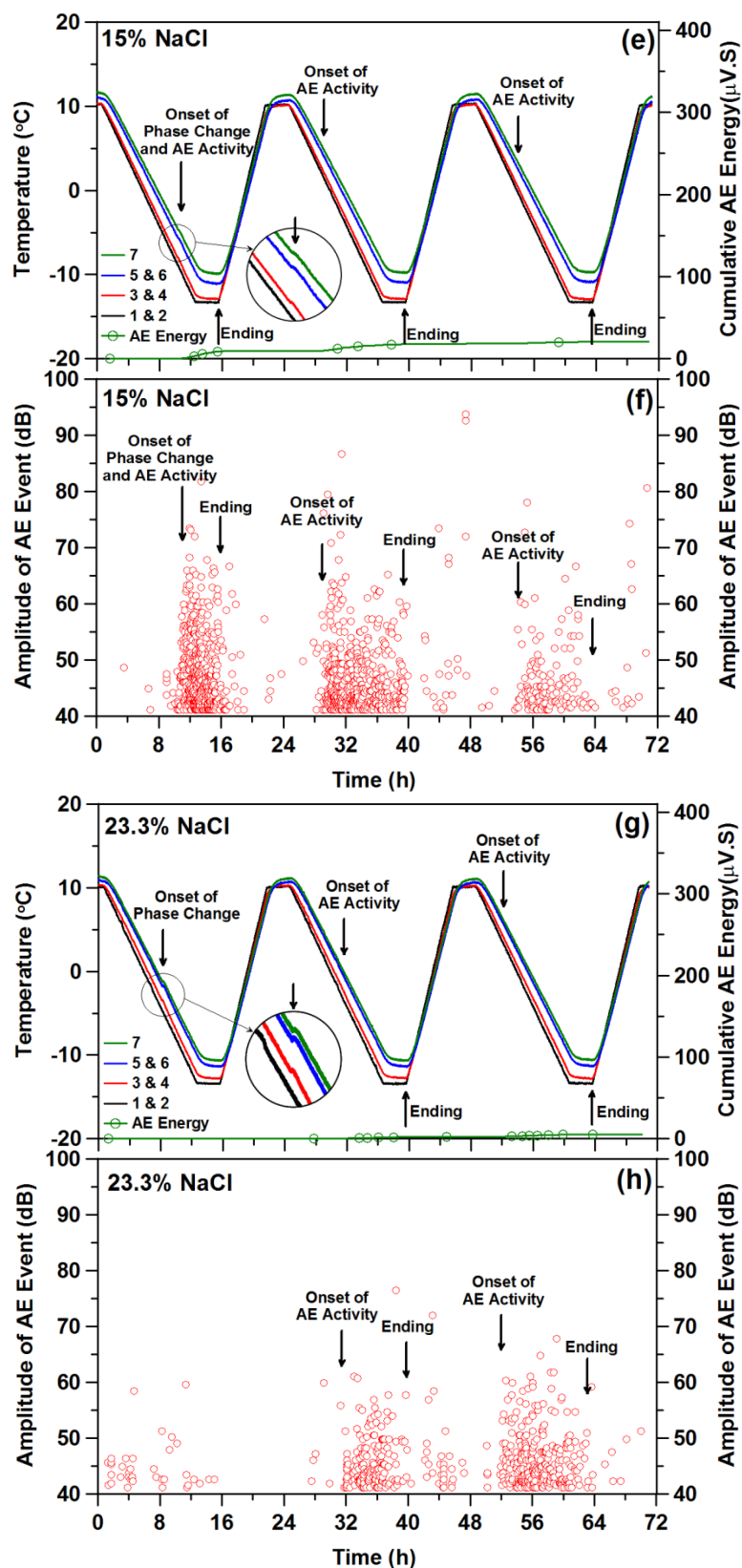
287

288

289
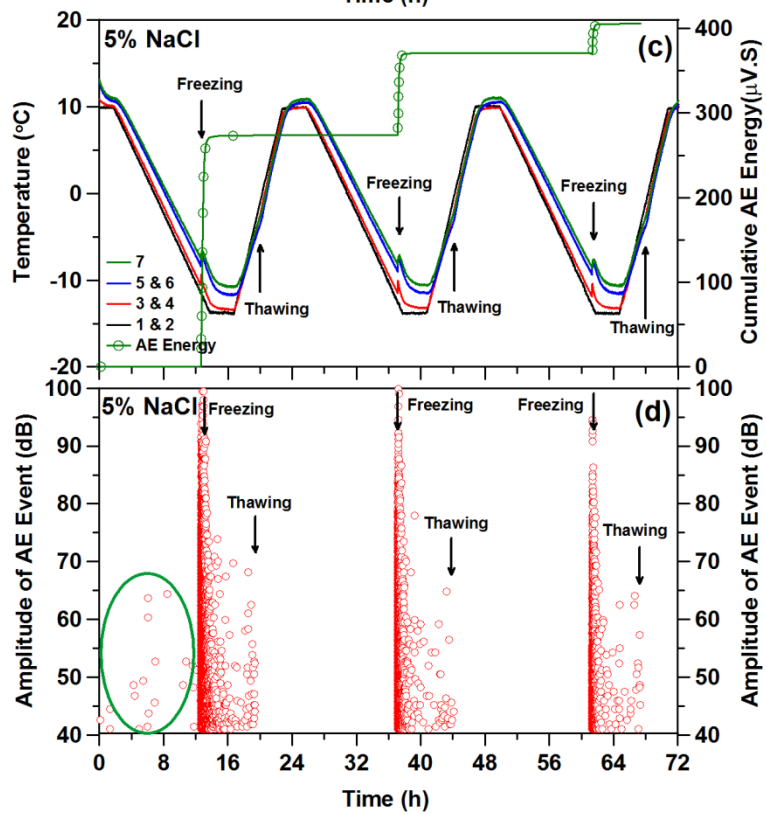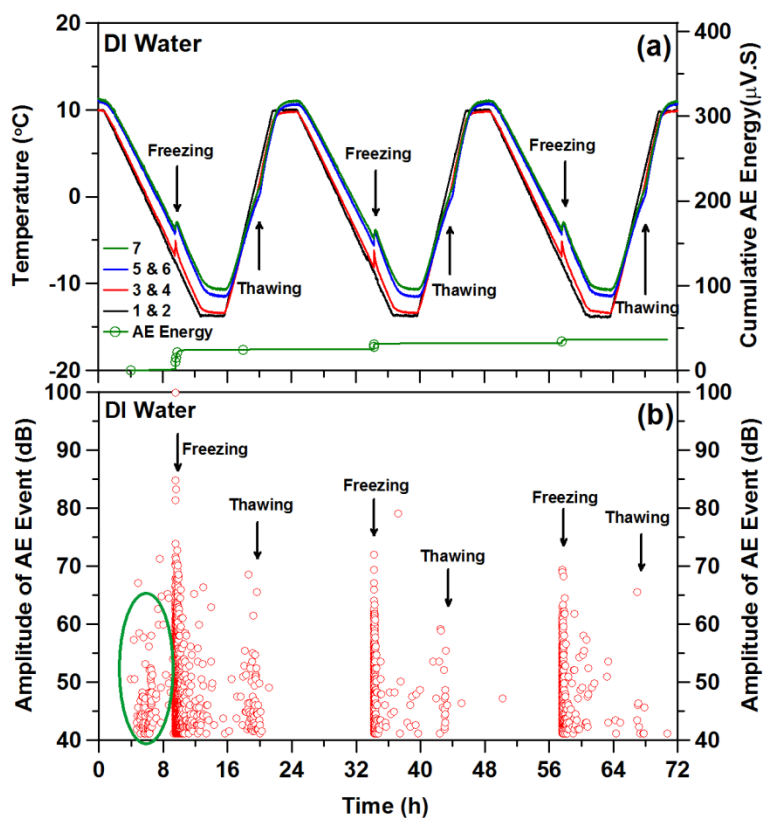
290
291 **FIGURE 2 Temperature at different locations, total cumulative acoustic energy, and amplitude of AE events**
292 **versus time during freeze-thaw cycles for specimens saturated with 0%, 5 %, 15 %, and 23.3 % NaCl**
293 **solutions.**

294   Figure 3 shows the heat flows (i.e., ΔQ_{Sample}) as a function of temperature. For specimens
295 containing 0 % and 5 % NaCl solutions, a large exothermic peak is seen during cooling
296 corresponding to the freezing point of water or NaCl solution (Figure 3a and 3b). According to
297 the temperature associated with this peak, solution in mortar is undercooled approximately 5 °C
298 to 7 °C with respect to its liquidus point from the NaCl solution phase diagram. For specimens
299 containing 15 % and 23.3 % NaCl solution, a small unexpected exothermic peak (associated with
300 an unexpected temperature jump) can be seen during cooling and became larger with an increase
301 in salt concentration (Figure 3c and 3d).
302   During the heating process, an endothermic peak was observed for 0 % and 5 %
303 concentrations due to the thawing of ice in contact with the pore solution, while no such peak
304 was seen for 15 % and 23.3 %, indicating that no thawing occurred in these latter two systems. It
305 should be also mentioned that no unexpected exothermic behavior was observed in cooling at
306 subsequent cycles showing that this action might be irreversible, however, AE activity was
307 observed in subsequent cycles which can represent the accumulation of the unexpected phase in
308 the following cycles. Table 2 shows the freeze-thaw temperature associated with the
309 exothermic/endothermic events detected for mortar specimens. While the freezing point was
310 undercooled, the thawing point matched exactly with the liquidus line of the aqueous NaCl phase
311 diagram.

312
313   **TABLE 2 Freezing and Thawing Temperatures at Bottom Surface of Specimens for the Three cycles**

NaCl Concentration	Freezing temperature (ºC)			Thawing temperature (ºC)		
(%)	1st Cycle	2nd Cycle	3rd Cycle	1st Cycle	2nd Cycle	3rd Cycle
0	-5.8	-7.1	-5.9	0.0	0.0	0.0
5	-9.6	-10.5	-10.9	-3.1	-3.2	-3.4
15	-7.0[*]	ND[**]	ND	ND	ND	ND
23.3	-2.5[*]	ND	ND	ND	ND	ND

314 * Temperature associated with the unexpected phase change
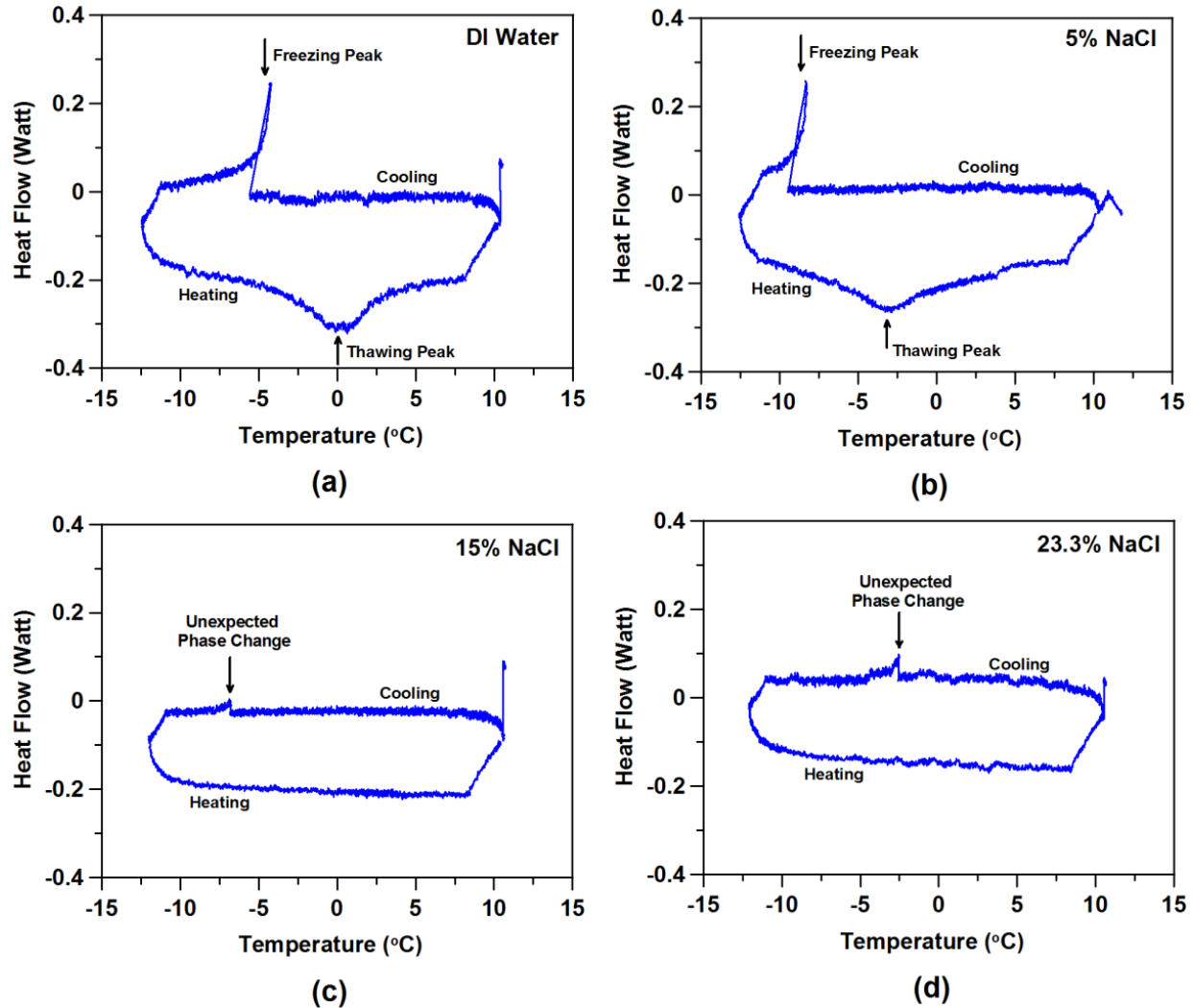315 ** ND = Not detected
316

317
318 **FIGURE 3 Heat flow inward/outward of mortar specimen versus temperature for first cycle of freeze-thaw**
319 **for mortar specimens saturated with (a deionized water; (b) 5% NaCl solution; (c) 15 % NaCl solution; and,**
320 **(d) 23.3 % NaCl solution.**

321

322   The relative dynamic modulus (E_t/E_o), the ratio of the dynamic modulus after a freeze
323 and thaw test to the dynamic modulus before the test) was used to assess the damage level of the
324 specimens as a result of freezing and thawing. The damage parameter (D) can be computed using
325 Equation 5.

$$D = 1 - \frac{E_t}{E_o} = 1 - (\frac{V_t}{V_o})^2 \tag{5}$$

326

327 where E_o and V_o are respectively dynamic elastic modulus and average pulse velocity before a
328 freeze and thaw test; and E_t, V_t are respectively dynamic elastic modulus and average pulse
329 velocity after the freeze and thaw test. An average pulse velocity was calculated before and after
330 freeze-thaw testing for each specimen. The damage index (D) and the total cumulative AE
331 energy for mortar specimens are shown in Figure 4a. Despite a smaller AE activity and less total
332 cumulative AE energy for 15 % and 23.3% specimens, a considerable damage index (change in
333 wave velocity) was observed for these specimens. This may indicate that the formation of an

334 unexpected phase change (i.e., not ice formation) led to a premature deterioration or that other
335 damage mechanisms are present. For specimens saturated by 5 % and 15 % NaCl solution,
336 relatively greater damage was observed after three cycles of freeze-thaw in comparison to
337 damage measured for specimens saturated by 0 % and 23.3 % NaCl solution. Greater damage in
338 specimens saturated by 5 % and 15% NaCl solutions may be attributed to the critical damage
339 caused by the combination of ice formation, osmotic pressure, and unexpected phase change
340 formation. Figure 4b indicates the crack pattern for the mortar specimen saturated with 15 %
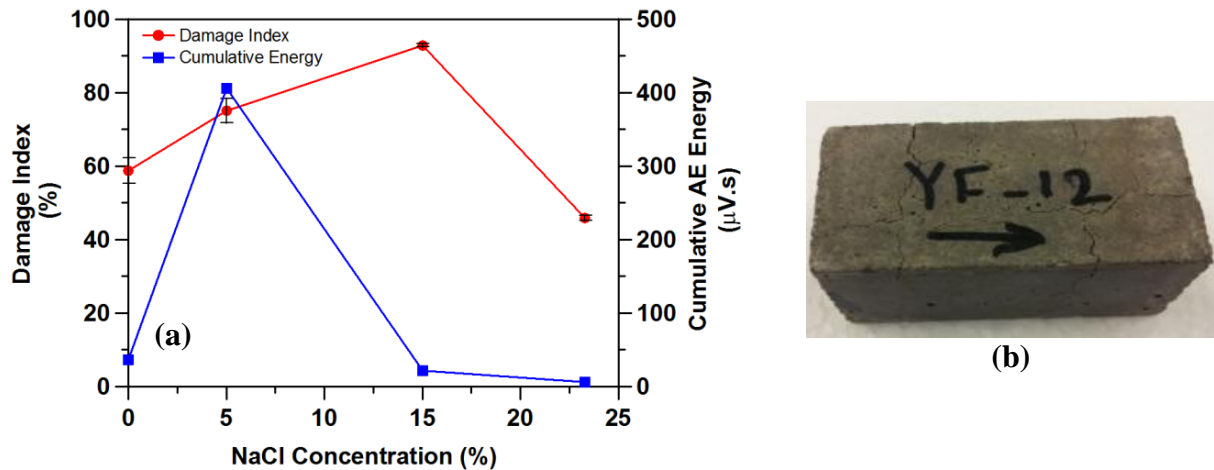341 NaCl solution after three cycles of freeze-thaw.

342

FIGURE 4 a) Cumulative acoustic energy and damage parameter for specimens after three cycles of freeze/thaw, b) crack pattern on the surface of the mortar specimen saturated with 15 % NaCl solution after three cycles of freeze-thaw testing (the error bars indicate ± one standard deviation for four replicates of pulse velocity testing).

347

Low Temperature Differential Scanning Calorimetry (LT-DSC)

349 Figure 5 compares the LT-DSC heat flow behavior for different specimens during heating as a
350 function of temperature. As expected, two endothermic peaks corresponding to eutectic melting
351 and ice thawing were observed for the NaCl solution. The eutectic and liquidus peaks for NaCl
352 solution are shown in Figure 6a as the salt concentration increases. Calcium hydroxide powder
353 showed almost the same trend as NaCl solution except for the high concentration case (Figure
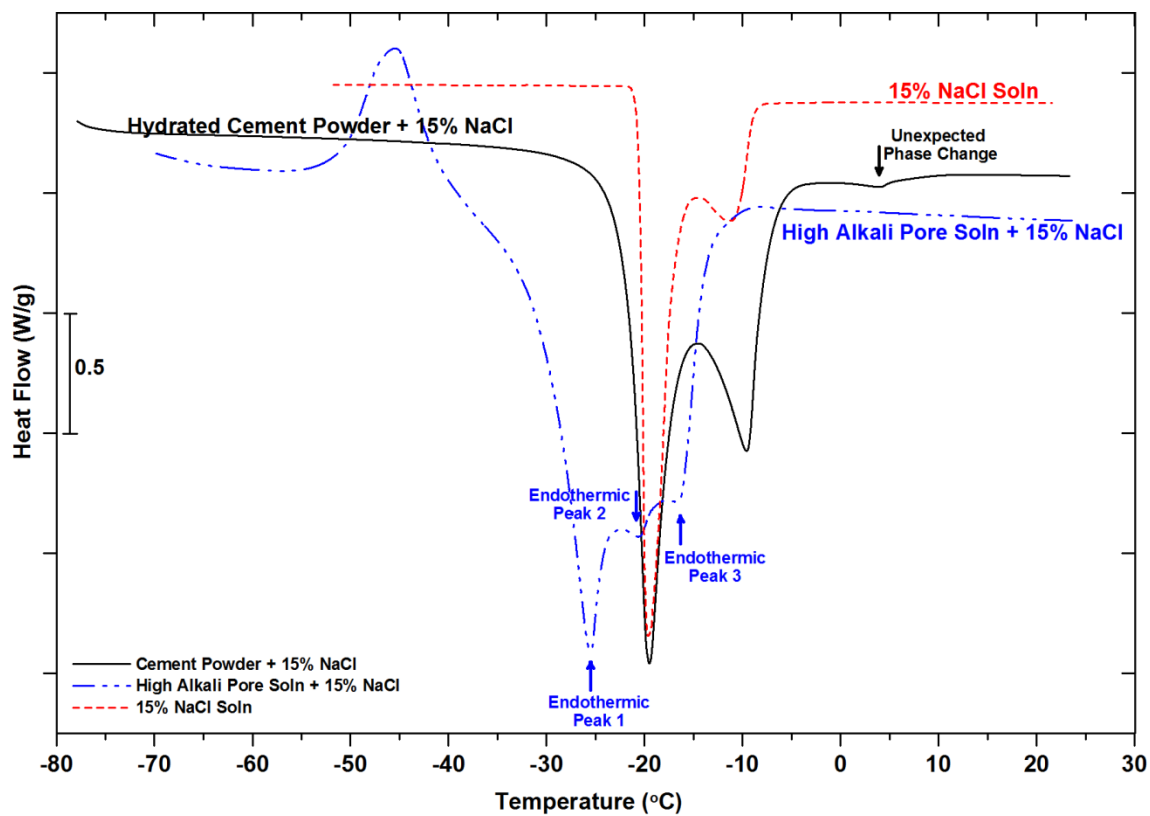354 6d); it seems that calcium hydroxide changes the eutectic concentration of NaCl solution.

355

356
357   **FIGURE 5 Heat flow during heating versus temperature for 15% NaCl solution, high alkali pore solution**
358   **containing 15% NaCl salt, and cement powder containing 15% NaCl solution (by mass).**
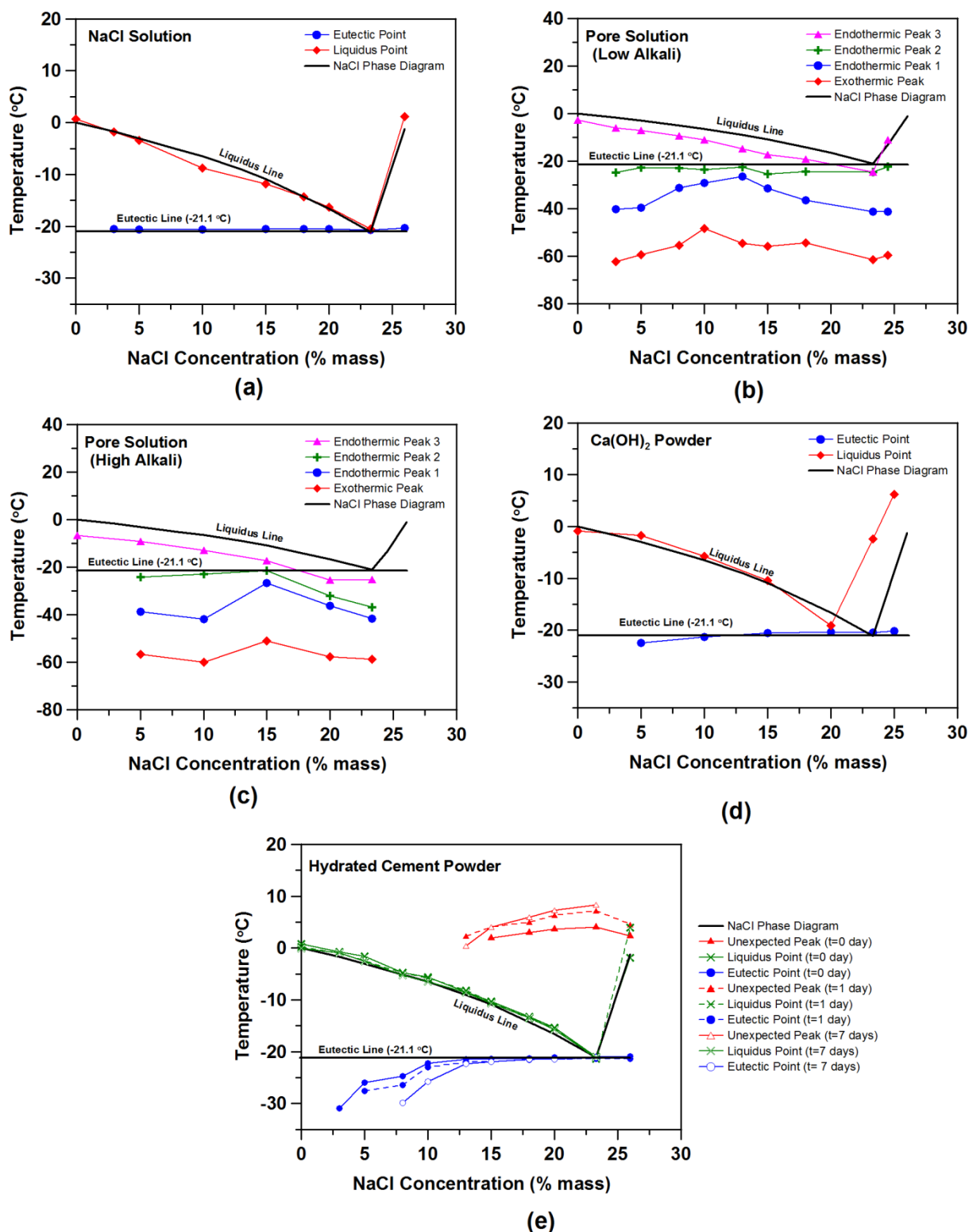359

FIGURE 6 Comparison of temperatures associated with different exotherms/endotherms observed in this study with aqueous NaCl phase diagram as a function of NaCl concentration for: a) NaCl solution, b) low alkali pore solution containing NaCl salt, c) high alkali pore solution containing NaCl salt, d) calcium hydroxide powder containing NaCl solution, and e) hydrated cement powder in different ages after mixing with NaCl solution.

Pore solutions behaved quite differently than NaCl solution and three endothermic behaviors were observed, with one exothermic peak at an onset temperature near -60 °C (Figure 5). The exothermic peak might correspond to experimental error due to the formation of the eutectic composition in heating instead of cooling. Figures 6b and 6c show the comparison of temperatures corresponding to these exothermic and endothermic behaviors with a classic NaCl solution phase diagram. For pore solution, it seems that the liquidus temperature (i.e., endothermic peak 3) for NaCl solution is depressed, while the eutectic temperature (i.e., endothermic peak 2 or formation of $NaCl \cdot 2H_2O$) remains close to -21.1 °C. The endothermic peak 1 may be attributed to the formation of $NaOH \cdot 7H_2O$ (transition temperature at -28.0 °C), respectively *(30)*.

Figure 6e indicates the temperature associated with different endotherms observed for hydrated cement powder containing NaCl solution during heating for different ages after mixing. The liquidus points for hydrated cement powder are similar to the aqueous NaCl liquidus line, while a different behavior is seen for the eutectic points. At higher concentrations of NaCl solution, the eutectic data are in good agreement with the NaCl solution eutectic line. At lower concentrations, however, eutectic temperatures are depressed to a lower temperature between the formation of $NaCl \cdot 2H_2O$ and $NaOH \cdot 7H_2O$, with transition temperatures of -21.1 °C and -28.0 °C, respectively. It should be mentioned that increasing the age after mixing, the eutectic temperature disappears at lower concentrations and becomes closer to that of $NaOH \cdot 7H_2O$. This may be attributed to consumption of chloride ions (Cl^-) due to binding and formation of Friedel's/Oxychloride/Kuzel's salt and concurrent release of sodium ions (Na^+) that can have an ionic bond with hydroxyl ions (OH^-).

Again, as observed in the AE-LGCC experiment, the unexpected phase transition was observed for hydrated cement powder whose temperature (associated with maximum absolute value of heat flow peak) was found to be between 0 °C and 8 °C. It should be mentioned that 5 °C to 7 °C undercooling should be considered to have a better comparison with AE-LGCC results as the unexpected phase change was observed only in cooling process in LGCC. Increasing the salt concentration, the temperature associated with the unexpected phase change increases. In addition, the unexpected phase change was observed to occur for a larger concentration range with increasing age. In other words, it was observed for a 13 % NaCl solution concentration after 1 d, while it was not seen immediately after mixing or t=0 d (Figure 6e). This can illustrate that the formation of alternative phases progresses during time. The source of this phase may be related to reactions of NaCl with cement hydration products and the formation of Friedel's/Oxychloride/Kuzel's salt; it may also be attributed to the dissolution of calcium hydroxide within the interfacial transition zone (ITZ) or NaCl changing the microstructure of cement hydration products *(9–14)*. More research is needed (including x-ray diffraction at low temperature) to understand the additional phase(s) observed in this study.

CONCLUSIONS

In this paper, the freeze-thaw behavior of cementitious mortar containing varying deicing salt concentrations was investigated using acoustic emission. While the conventional interpretation of a phase diagram would suggest no damage developing in the mortars saturated by higher concentrations of NaCl solutions (as ice has not formed) damage was detected. To investigate potential causes of this damage, low temperature calorimetry was used and was able to detect an additional phase forming at higher concentrations of NaCl in cementitious systems that does not form when only the NaCl-water systems or NaCl-pore solution systems are tested. The

composition of this additional phase is not clear; however, it may be related to reactions with cement hydration products that result in the formation of Friedel's/Oxychloride/Kuzel's salt, dissolution of calcium hydroxide, and changes in the microstructure of cement hydration products. It appears that the formation of an additional phase at the temperature above the liquidus line produces an expansion that results in some cracking and damage development that can be detected with acoustic emission. This may provide one explanation for damage that occurs in freezing and thawing when high concentration salt solutions are used even if actual freezing of the pore solution is not occurring; however, there may be other causes as well. Research is underway to better understand the products being formed at these higher concentrations.

REFERENCES

1.   Shi, X., Y. Liu, M. Mooney, B. Hubbard, L. Fay, and A. Leonard. *Effect of Chloride-based Deicers on Reinforced Concrete Structures*. WA-RD 741.1. Washington State Department of Transportation, 2010, p. 86.

2.   Li, W., W. Sun, and J. Jiang. Damage of concrete experiencing flexural fatigue load and closed freeze/thaw cycles simultaneously. *Construction and Building Materials*, Vol. 25, No. 5, May 2011, pp. 2604–2610.

3.   John Valenza. *Mechanism for salt scaling*. Princeton University, 2005.

4.   Yoon, D.-J., W. J. Weiss, and S. P. Shah. Detecting the extent of corrosion with acoustic emission. *Transportation research record*, 2000, pp. 54–60.

5.   Powers, T. A working hypothesis for further studies of frost resistance of concrete. In: *Journal of the American Concrete Institute, No. 41,* Portland Cement Association, Detroit, Michigan,1945, pp. 245–272.

6.   Powers, T. C. The physical structure and engineering properties of concrete. *Research department bulletin, Portland Cement Association*, Vol. 90, 1958, p. 27 pages.

449 7. Kaufmann, J. *Experimental identification of damage mechanisms in cementitious porous*
450 *materials on phase transition of pore solution under deicing salt attack*. École
451 polytechnique fédérale de Lausanne (EPFL), 2000.

452 8. Mehta, P. K., and P. J. Monteiro. *Concrete: microstructure, properties, and materials*.
453 McGraw-Hill, New York, 2005.

454 9. Sutter, L., K. Peterson, S. Touton, T. Van Dam, and D. Johnston. Petrographic evidence of
455 calcium oxychloride formation in mortars exposed to magnesium chloride solution.
456 *Cement and Concrete Research*, Vol. 36, No. 8, Aug. 2006, pp. 1533–1541.

457 10. Mesbah, A., M. François, C. Cau-dit-Coumes, F. Frizon, Y. Filinchuk, F. Leroux, J.
458 Ravaux, and G. Renaudin. Crystal structure of Kuzel's salt
459 3CaO·Al2O3·1/2CaSO4·1/2CaCl2·11H2O determined by synchrotron powder diffraction.
460 *Cement and Concrete Research*, Vol. 41, No. 5, May 2011, pp. 504–509.

461 11. Sutter, L., K. Peterson, G. Julio-Betancourt, D. Hooton, T. V. Dam, and K. Smith. *The*
462 *deleterious chemical effects of concentrated deicing solutions on Portland cement*
463 *concrete*. SD2002-01-F. Final report for the South Dakota Department of Transportation,
464 2008, p. 57.

465 12. Collepardi, M., L. Coppola, and C. Pistolesi. Durability of concrete structures exposed to
466 CaCl2 based deicing salts. In: *Durability of Concrete ACI SP-145, 3rd CANMET/ACI*
467 *International Conference,* American Concrete Institute, 1994, pp. 107-120.

468 13. Pigeon, M., and M. Regourd. The effects of freeze-thaw cycles on the microstructure of
469 hydration products. *Durability of building materials*, Vol. 4, No. 1, 1986, pp. 1–19.

470 14. Shi, X., L. Fay, M. M. Peterson, and Z. Yang. Freeze–thaw damage and chemical change
471 of a portland cement concrete in the presence of diluted deicers. *Materials and Structures*,
472 Vol. 43, No. 7, Oct. 2009, pp. 933–946.

473 15. Li, W., M. Pour-Ghaz, J. Castro, and J. Weiss. Water absorption and critical degree of
474 saturation relating to freeze-thaw damage in concrete pavement joints. *Journal of*
475 *Materials in Civil Engineering*, Vol. 24, No. 3, Mar. 2012, pp. 299–307.

476 16. Yang, Z., W. J. Weiss, and J. Olek. Water transport in concrete damaged by tensile
477 loading and freeze–thaw cycling. *Journal of Materials in Civil Engineering*, Vol. 18, No.
478 3, Jun. 2006, pp. 424–434.

479 17. Park, W. S., and J. H. Lee. Evaluation of freeze-thaw damage in concrete by one-sided
480 stress wave velocity measurement technique. *Key Engineering Materials*, Vol. 270-273,
481 2004, pp. 1604–1609.

18.   Ohtsu, M. Nondestructive evaluation of damaged concrete due to freezing and thawing by elastic-wave method. *Journal of Advanced Concrete Technology*, Vol. 3, No. 3, 2005, pp. 333–341.

19.   Shimada, H., K. Sakai, and G. G. Litvan. Acoustic emissions of mortar subjected to freezing and thawing. In: *Second international Conference on Durability of Concrete,* Montreal, Canada, 1991, pp. 263-278.

20.   Qian, Y., Y. Farnam, and J. Weiss. Using acoustic emission to quantify freeze-thaw damage of mortar saturated with NaCl solutions. In: *International Conference on Sustainable Construction Materials & Technologies,* Kyoto, Japan, 2013, pp. 1-10.

21.   Farnam, Y., D. Bentz, A. Sakulich, D. Flynn, and J. Weiss. Measuring Freeze and Thaw Damage in Mortars Containing Deicing Salt Using a Low Temperature Longitudinal Guarded Comparative Calorimeter and Acoustic Emission (AE-LGCC). *Advances in Civil Engineering Materials (Under Review).*

22.   Litvan, G. Frost action in cement in the presence of de-icers. *Cement and Concrete Research*, Vol. 6, No. September 1974, 1976, pp. 351–356.

23.   Beddoe, R., and M. Setzer. A low-temperature DSC investigation of hardened cement paste subjected to chloride action. *Cement and Concrete Research*, Vol. 18, No. 2, 1988, pp. 249–256.

24.   Beddoe, R., and M. Setzer. Phase transformations of water in hardened cement paste, a low-temperature DSC investigation. *Cement and Concrete Research*, Vol. 20, No. 2, 1990, pp. 236–242.

25.   Han, B., J. H. Choi, J. Dantzig, and J. C. Bischof. A quantitative analysis on latent heat of an aqueous binary mixture. *Cryobiology*, Vol. 52, No. 1, Feb. 2006, pp. 146–51.

26.   *ASTM C305 - Standard practice for mechanical mixing of hydraulic cement pastes and mortars of plastic consistency*. ASTM International, West Conshohocken, PA, 2012.

27.   *ASTM C1645/C1645M – Standard Test Method for Freeze-thaw and De-icing Salt Durability of Solid Concrete Interlocking Paving Units*. ASTM International, West Conshohocken, PA, 2011.

28.   Bentz, D. P. A virtual rapid chloride permeability test. *Cement and Concrete Composites*, Vol. 29, No. 10, Nov. 2007, pp. 723–731.

29.   Scherer, G. Crystallization in pores. *Cement and Concrete research*, Vol. 29, No. December 1998, 1999, pp. 1347–1358.

30.   Purdon, F. F., and V. W. Slater. *Aqueous Solution and The Phase Diagram*. Butler & Tanner Ltd., Frome and London, London, Great Britain, 1946.